www.sciencemag.org/cgi/content/full/336/6086/1280/DC1

Supplementary Materials for

Quantum Information Storage for over 180 s Using Donor Spins in a 28Si "Semiconductor Vacuum"

M. Steger, K. Saeedi, M. L. W. Thewalt,* J. J. L. Morton, H. Riemann, N. V. Abrosimov, P. Becker, H.-J. Pohl

*To whom correspondence should be addressed. E-mail: thewalt@sfu.ca

Published 8 June 2012, *Science* **336**, 1280 (2012)
DOI: 10.1126/science.1217635

This PDF file includes:

Materials and Methods

The sample used here measured 11.8 x 4.5 x 1.7 mm^3 and was cut from segment Si28-10Pr11.02.2 located near the seed end of the Avogadro crystal (*4*). It was etched in HF/HNO_3, which is essential to remove surface damage, which would otherwise strain the sample and broaden the D^0X transitions. The sample is enriched to 99.995% ^{28}Si, and contains 46 ppm ^{29}Si, $5x10^{11}$ cm^{-3} P, $5x10^{13}$ cm^{-3} B, $<10^{13}$ cm^{-3} O and $<10^{14}$ cm^{-3} C.

Some aspects of the experimental apparatus were described in our preliminary study (*19*), while the improvements discussed here are detailed in Figure S1. The sample sits loosely in a cavity in contact with the liquid He coolant. The temperatures given here are those of the He bath as determined from the He vapor pressure. The sample is centered between the polefaces of the iron-core electromagnet which supplies the static magnetic field B~845 G. For stabilization purposes, B is monitored at the center of one of the polefaces with a Gaussmeter. While the stated value of ~845 G is corrected for the difference of B between the pole face and sample location, the exact field at the sample is not known. As outlined previously (*19*), the $RF_\uparrow$ and $RF_\downarrow$ resonance frequencies were determined as a function of B to ensure that we were working at B_0, the field at which $RF_\downarrow$ is at a minimum and $RF_\uparrow$ is at a maximum, greatly relaxing the homogeneity and stability constraints on B. The exact resonance frequencies at B_0 (*19*) and the Si band gap energy (*33*), and thus the D^0X transition energies, have a small dependence on T and He vapor pressure, which had to be taken into account when changing the sample temperature.

Optical excitation is provided by three lasers through computer-controlled shutters. The above-gap 1047 nm radiation comes from a diode-pumped Nd:YLF laser, with a typical intensity at the sample of 0.5 $mWcm^{-2}$. The two resonant excitation sources are tuneable, single frequency Yb-doped distributed feedback fibre lasers, followed by Yb-doped fibre amplifiers capable of providing up to 1 W of output power. Typical resonant laser powers at the sample were 10 $mWcm^{-2}$ for the readout laser and 250 $mWcm^{-2}$ for the polarizing laser. The resonant lasers were locked and scanned with respect to a stabilized reference cavity, which was itself locked to a frequency stabilized HeNe laser. The NMR sequences occur with the laser shutters closed, and efforts were made to minimize background light falling on the sample under these conditions.

The RF magnetic field B_1 was orthogonal to B, and produced by a 10 turn Cu coil with an approximate cross section of 20x40 mm^2, and length of 40 mm. The coil was matched to 50 ohms by a tuning circuit external to the He dewar at 58.75 MHz, half way between the ~55.847 MHz $RF_\uparrow$ and ~61.677 MHz $RF_\downarrow$ frequencies. The synthesizers used to generate $RF_\uparrow$ and $RF_\downarrow$ were driven by a 10 MHz Rb clock to improve frequency stability. A low RF power of ~60 mW was used in these experiments, resulting in π pulse lengths of ~500 μs.

The apparatus was still configured to collect any resonantly generated D^0X luminescence from the sample, as used previously (*17-19*) to monitor D^0X creation, but the low ^{31}P concentration in the present sample made this luminescence almost

impossible to detect. Instead, the change in conductivity resulting from Auger electrons was detected using a noncontact, capacitive photoconductivity approach. This noncontact approach eliminated any possibility of straining the sample, and also eliminated the need for ohmic contacts. As shown in Figure S1, the sample was an element in a parallel plate capacitor, with no direct electrical contact between the sample and electrodes. A 114 kHz sine wave, with amplitude of 20 V PP, was applied to one electrode, and the other electrode was connected to a high gain, high impedance amplifier. A phase-shifted and attenuated signal was coupled to the same input through a 1 pF capacitor, forming an impedance bridge which allowed the signal coupled through the sample to be cancelled under any particular illumination conditions. The out-of-balance bridge signal was then fed to a lock-in amplifier, with the output being the photoconductive signal of interest. For the collection of spectra, as in Figure 1, the readout laser was additionally chopped at 40 Hz, and a second lock-in amplifier was used to process the photoconductive signal and detect only the component resulting from the chopped readout laser.

Supplementary Text

Photoneutralization

At the low impurity concentrations used here, donor-acceptor-pair recombination is very slow (*34*). After illumination with above-gap light the majority of the donors and acceptors will remain neutral for very long times in the absence of light capable of photoionizing the impurities, although it is possible that some recombination, and thus loss of D^0 population, takes place during the long dark times needed to measure T_{2n}. At 4.2 K we obtained resonant D^0X hyperpolarization and AEDMR signals for hours after only a brief photoneutralization, but as the temperature was lowered these signals rapidly weakened, requiring the application of a small amount of 1047 nm radiation during the polarization and readout periods. We believe that this change with temperature resulted from the formation of overcharged acceptor centers (A^+) on the excess boron, since the problem was absent in n-type material, and the A^+ centers have a very small binding energy (*35*), explaining the temperature dependence. Note that the lasers tuned to lines 4 and 6 will, in addition to any resonant D^0X creation, also cause a very weak nonresonant photoionization of all D^0 and A^0 via their photoionization continua. The A^+ formed by free hole capture on A^0 would compete with D^+ in capturing e^-, forming acceptor bound excitons (A^0X), and then via Auger recombination A^- and h^+, resulting eventually in all of the donors becoming ionized in the absence of above-gap excitation.

Comparison of new hyperpolarization method with previous scheme

The necessity of having above-gap excitation at 1047 nm to achieve donor photoneutralization in the present p-type sample required changes to the previous method of donor hyperpolarization (*18*), which was used in the preliminary study of optically hyperpolarized/detected NMR of ^{31}P in n-type ^{28}Si (*19*). In comparison to our new method as outlined in Figure 1 (**B**), the previous scheme used only the high power polarizing laser tuned to line 6, Auger-ionizing donors in state $|2\rangle$, with some of the thermalized electrons being recaptured with opposite spin into $|3\rangle$. D^0 in $|1\rangle$ and $|4\rangle$ transfer via the W and R relaxation processes, which are very slow in the dark but more rapid in the presence of free carriers, to $|2\rangle$ where they are rapidly ionized. While this

method could give $P_n = 0.76$ for n-type material in the absence of above-gap excitation (*18*), with the present p-type sample and the necessary above-gap excitation the maximum nuclear polarization achievable with the previous method was $P_n = 0.35$. The reduced nuclear (and electronic) polarization in the presence of above-gap excitation result both from the increased speed of relaxation processes induced by the free carriers, as well as from the Auger ionization of D^0 in all four hyperfine states by the formation of D^0X via the random capture of free excitons onto D^0.

The $P_n = 0.90$ achieved by the new hyperpolarization scheme is a major improvement on these earlier results. In addition, the new scheme also shortened the polarization time constant under these conditions from ~1 s to 100 ms. Taken together, this method is much faster and more effective than any previous (*7, 11, 19*) nuclear polarization scheme for impurities in semiconductors. Note that the nonresonant optical hyperpolarization method reported (*11, 20*) for donor nuclear spins would not be useful under the present conditions, since it requires a high magnetic field to produce a large equilibrium electron polarization, which is transferred to the nuclear spins.

Quantum process tomography

The density matrix of a quantum state can be experimentally uncovered through a number of repeated measurements in different bases (requiring multiple copies, or preparations, of the state). This is known as quantum state tomography, and can be performed in a variety of different ways (*36*). Having established a method for experimentally determining quantum states, one can also characterise the nature of a *process* applied to a quantum state, be it a unitary operation such as a coherent manipulation or a non-unitary one such as relaxation or decoherence. This requires preparing a number of known initial states (characterized by state tomography), applying the process, and then measuring the outcome. For a single qubit, we prepare four input states (corresponding to $|0\rangle$, $|1\rangle$, $|+\rangle$ and $|i\rangle$, or in terms of a spin magnetization, +Z, –Z, +X and +Y), and use the resulting output states to compose a process matrix, in the basis of the operators **I**, **X**, **Y**, **Z** (*36*). In practice, the initial state preparation is imperfect, so we perform the tomography of i) the state preparation process, χ_{prep}, and ii) the combined process of state preparation process followed by dynamical decoupling, χ_{total}. We can then use these to compose the process describing the dynamical decoupling alone, χ_{dd}. In summary:

$$\chi_{total}(\rho) = \chi_{dd}(\chi_{prep}(\rho)) \qquad \text{(S.1)}$$

In Figure S2 we show the quantum process matrix, χ_{dd}, for both 16 s and 112 s of dynamical decoupling, as well as some ideal process matrices to guide the interpretation of what we observe (namely, those for the Identity operator, pure dephasing, and relaxation to a maximally mixed state). After 16 s, the process matrix has amplitudes <0.02 in all elements apart from $|\mathbf{I}\rangle\langle\mathbf{I}|$, showing a good approximation to the Identity operator, as desired for state preservation. The next greatest element is $|\mathbf{Z}\rangle\langle\mathbf{Z}|$, corresponding to pure dephasing. After 112 s, we see that the Identity component has decreased, indicating the corruption of the initial state. Although the $|\mathbf{Z}\rangle\langle\mathbf{Z}|$ component is greatest, suggesting that there is some dephasing, the considerable amplitude of $|\mathbf{X}\rangle\langle\mathbf{X}|$

and $|\mathbf{Y}\rangle\langle\mathbf{Y}|$ is consistent with some relaxation to a maximally mixed state. Given that the nuclear T_1 is expected to be extremely long (hours) under these conditions, we attribute this to pulse imperfections, although as discussed previously there may also be some loss of D^0 due to ionization. We can therefore conclude that if pulse errors are reduced, for example using composite pulse sequences, that the storage time in the ^{31}P nuclear spin could be even longer.

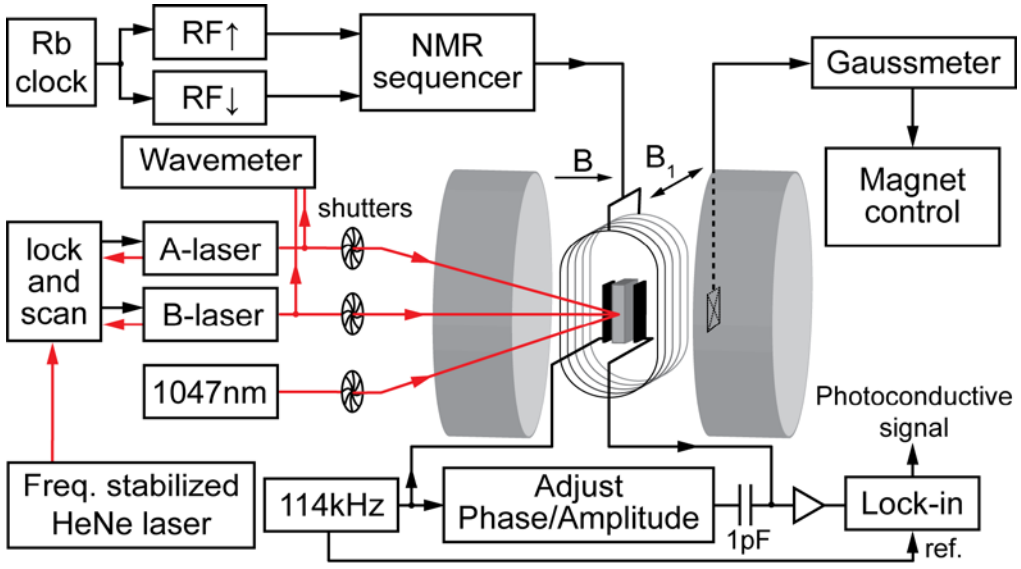

Fig. S1.

A schematic of the hyperfine-resolved optical hyperpolarization and photoconductive readout apparatus used to detect NMR of dilute ^{31}P in highly enriched ^{28}Si.

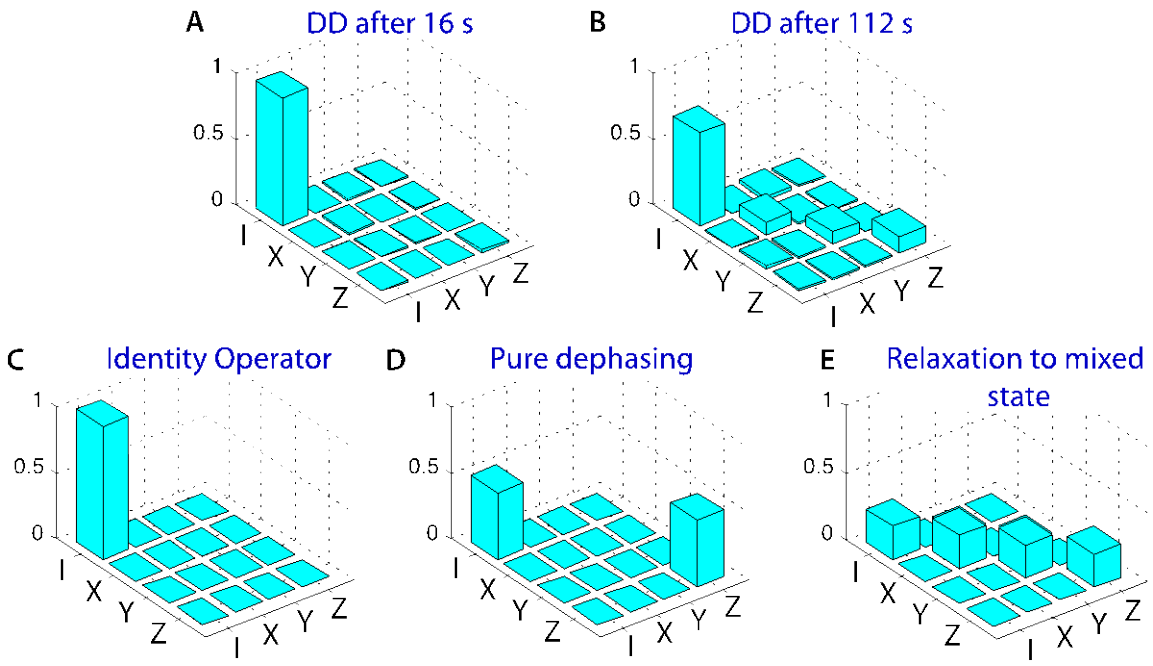

Fig. S2

Quantum process matrices. The application of dynamical decoupling to the nuclear spin state for a duration of (**A**) 16 s and (**B**) 112 s is characterised by the process matrices shown. For reference, we show the quantum process matrix for (**C**) the ideal Identity operator, (**D**) a pure dephasing process, and (**E**) a relaxation process, which drives the system to a mixed state. The experimentally observed processes can be understood in terms of contributions from these three processes.

References and Notes

1. D. Deutsch, Quantum theory, the Church-Turing principle and the universal quantum computer. *Proc. R. Soc. London Ser. A* **400**, 97 (1985). doi:10.1098/rspa.1985.0070

2. J. P. Home *et al.*, Complete methods set for scalable ion trap quantum information processing. *Science* **325**, 1227 (2009); 10.1126/science.1177077. doi:10.1126/science.1177077 Medline

3. J. J. L. Morton, D. R. McCamey, M. A. Eriksson, S. A. Lyon, Embracing the quantum limit in silicon computing. *Nature* **479**, 345 (2011). doi:10.1038/nature10681 Medline

4. P. Becker, H.-J. Pohl, H. Riemann, N. V. Abrosimov, Enrichment of silicon for a better kilogram. *Phys. Status Solidi A* **207**, 49 (2010). doi:10.1002/pssa.200925148

5. T. D. Ladd *et al.*, Quantum computers. *Nature* **464**, 45 (2010). doi:10.1038/nature08812 Medline

6. B. E. Kane, A silicon-based nuclear spin quantum computer. *Nature* **393**, 133 (1998). doi:10.1038/30156

7. J. J. L. Morton *et al*., Solid-state quantum memory using the ^{31}P nuclear spin. *Nature* **455**, 1085 (2008). doi:10.1038/nature07295

8. D. R. McCamey, J. Van Tol, G. W. Morley, C. Boehme, Electronic spin storage in an electrically readable nuclear spin memory with a lifetime >100 seconds. *Science* **330**, 1652 (2010). doi:10.1126/science.1197931 Medline

9. S. Simmons *et al*., Entanglement in a solid-state spin ensemble. *Nature* **470**, 69 (2011). doi:10.1038/nature09696 Medline

10. A. M. Tyryshkin *et al*., Electron spin coherence exceeding seconds in high-purity silicon. *Nat. Mater.* **11**, 143 (2012). doi:10.1038/nmat3182 Medline

11. D. R. McCamey, J. van Tol, G. W. Morley, C. Boehme, Fast nuclear spin hyperpolarization of phosphorus in silicon. *Phys. Rev. Lett.* **102**, 027601 (2009). doi:10.1103/PhysRevLett.102.027601 Medline

12. H. Morishita *et al*., Electrical detection and magnetic-field control of spin states in phosphorus-doped silicon. *Phys. Rev. B* **80**, 205206 (2009). doi:10.1103/PhysRevB.80.205206

13. L. Dreher, F. Hoehne, M. Stutzmann, M. S. Brandt, Nuclear spins of ionized phosphorus donors in silicon. *Phys. Rev. Lett.* **108**, 027602 (2012). doi:10.1103/PhysRevLett.108.027602 Medline

14. A. Morello *et al*., Single-shot readout of an electron spin in silicon. *Nature* **467**, 687 (2010). doi:10.1038/nature09392 Medline

15. W. M. Witzel, M. S. Carroll, A. Morello, Ł. Cywiński, S. Das Sarma, Electron spin decoherence in isotope-enriched silicon. *Phys. Rev. Lett.* **105**, 187602 (2010). doi:10.1103/PhysRevLett.105.187602 Medline

16. M. Cardona, M. L. W. Thewalt, Isotope effects on the optical spectra of semiconductors. *Rev. Mod. Phys.* **77**, 1173 (2005). doi:10.1103/RevModPhys.77.1173

17. A. Yang *et al*., Optical detection and ionization of donors in specific electronic and nuclear spin States. *Phys. Rev. Lett.* **97**, 227401 (2006). doi:10.1103/PhysRevLett.97.227401 Medline

18. A. Yang *et al*., Simultaneous subsecond hyperpolarization of the nuclear and electron spins of phosphorus in silicon by optical pumping of exciton transitions. *Phys. Rev. Lett.* **102**, 257401 (2009). doi:10.1103/PhysRevLett.102.257401 Medline

19. M. Steger *et al*., Optically-detected NMR of optically-hyperpolarized ^{31}P neutral donors in ^{28}Si. *J. Appl. Phys.* **109**, 102411 (2011). doi:10.1063/1.3577614

20. T. Sekiguchi *et al*., Hyperfine structure and nuclear hyperpolarization observed in the bound exciton luminescence of Bi donors in natural Si. *Phys. Rev. Lett.* **104**, 137402 (2010). doi:10.1103/PhysRevLett.104.137402 Medline

21. T. D. Ladd, D. Maryenko, Y. Yamamoto, E. Abe, K. M. Itoh, Coherence time of decoupled nuclear spins in silicon. *Phys. Rev. B* **71**, 014401 (2005). doi:10.1103/PhysRevB.71.014401

22. C. Langer *et al*., Long-lived qubit memory using atomic ions. *Phys. Rev. Lett.* **95**, 060502 (2005). doi:10.1103/PhysRevLett.95.060502 Medline

23. A. Yang *et al*., Homogeneous linewidth of the ^{31}P bound exciton transition in silicon. *Appl. Phys. Lett.* **95**, 122113 (2009). doi:10.1063/1.3238268

24. W. Schmid, Auger lifetimes for excitons bound to neutral donors and acceptors in Si. *Phys. Status Solidi B* **84**, 529 (1977). doi:10.1002/pssb.2220840216

25. Materials and methods are available as supplementary materials on *Science* Online.

26. L. Viola, S. Lloyd, Dynamical suppression of decoherence in two-state quantum systems. *Phys. Rev. A* **58**, 2733 (1998). doi:10.1103/PhysRevA.58.2733

27. A. M. Tyryshkin *et al*., Dynamical decoupling in the presence of realistic pulse errors (2010); http://arxiv.org/abs/:1011.1903v2.

28. T. Gullion, D. B. Baker, M. S. Conradi, New, compensated Carr-Purcell sequences. *J. Magn. Reson.* **89**, 479 (1990). doi:10.1016/0022-2364(90)90331-3

29. G. Feher, E. A. Gere, Electron spin resonance experiments on donors in silicon. II. electron spin relaxation effects. *Phys. Rev.* **114**, 1245 (1959). doi:10.1103/PhysRev.114.1245

30. D. Sleiter *et al*., Quantum Hall charge sensor for single-donor nuclear spin detection in silicon. *New J. Phys.* **12**, 093028 (2010). doi:10.1088/1367-2630/12/9/093028

31. J. J. L. Morton, A silicon-based cluster state quantum computer (2009); http://arxiv.org/abs/0905.4008v1.

32. S. R. Schofield *et al*., Atomically precise placement of single dopants in si. *Phys. Rev. Lett.* **91**, 136104 (2003). doi:10.1103/PhysRevLett.91.136104 Medline

33. M. Cardona, T. A. Meyer, M. L. W. Thewalt, Temperature dependence of the energy gap of semiconductors in the low-temperature limit. *Phys. Rev. Lett.* **92**, 196403 (2004). doi:10.1103/PhysRevLett.92.196403 Medline

34. P. Dirksen, A. Henstra, W. Th. Wenckebach, An electron spin echo study of donor-acceptor recombination. *J. Phys. Condens. Matter* **1**, 7085 (1989). doi:10.1088/0953-8984/1/39/020

35. W. Burger, K. Lassmann, Energy-resolved measurements of the phonon-ionization of D^- and A^+ centers in silicon with superconducting-Al tunnel junctions. *Phys. Rev. Lett.* **53**, 2035 (1984). doi:10.1103/PhysRevLett.53.2035

36. U. Leonhardt, Quantum-state tomography and discrete Wigner function. *Phys. Rev. Lett.* **74**, 4101 (1995). doi:10.1103/PhysRevLett.74.4101 Medline

37. M. A. Nielsen, I. L. Chuang, *Quantum Computation and Quantum Information* Cambridge Univ. Press, Cambridge, 2000).